Chronic Dicer1 deficiency promotes atrophic and neovascular outer retinal pathologies in mice

Charles B. Wright[a,1], Hironori Uehara[b,1], Younghee Kim[c,d,3], Tetsuhiro Yasuma[a], Reo Yasuma[c,d], Shuichiro Hirahara[c,d], Ryan D. Makin[c,d,e], Ivana Apicella[c,d], Felipe Pereira[c,d,f], Yosuke Nagasaka[c,d], Siddharth Narendran[c,d,g], Shinichi Fukuda[c,d,h], Romulo Albuquerque[a,4], Benjamin J. Fowler[a], Ana Bastos-Carvalho[a], Philippe Georgel[i,j], Izuho Hatada[k], Bo Chang[l], Nagaraj Kerur[c,d], Balamurali K. Ambati[b], Jayakrishna Ambati[c,d,m,n], and Bradley D. Gelfand[c,d,o,2]

[a]Department of Ophthalmology and Visual Sciences, University of Kentucky, Lexington, KY 40506; [b]Department of Ophthalmology, Loma Linda University, Loma Linda, CA 92350; [c]Center for Advanced Vision Science, University of Virginia School of Medicine, Charlottesville, VA 22903; [d]Department of Ophthalmology, University of Virginia School of Medicine, Charlottesville, VA 22903; [e]Molecular and Cellular Basis of Disease Graduate Program, University of Virginia School of Medicine, Charlottesville, VA 22903; [f]Departamento de Oftalmologia e Ciências Visuais, Escola Paulista de Medicina, Universidade Federal de São Paulo, São Paulo 04039-032, Brazil; [g]Aravind Medical Research Foundation, Aravind Eye Care System, Madurai, Tamil Nadu 625020, India; [h]Department of Ophthalmology, University of Tsukuba, Ibaraki 305-8575, Japan; [i]Laboratoire d'ImmunoRhumatologie Moléculaire, INSERM UMR-S1109, LabEx Transplantex, Fédération de Médecine Translationnelle de Strasbourg, Université de Strasbourg, 67085 Strasbourg, France; [j]Fédération Hospitalo-Universitaire OMICARE, Université de Strasbourg, 67085 Strasbourg, France; [k]Laboratory of Genome Science, Biosignal Genome Resource Center, Institute for Molecular and Cellular Regulation, Gunma University, Maebashi 371-8512, Japan; [l]The Jackson Laboratory, Bar Harbor, ME 04609; [m]Department of Pathology, University of Virginia School of Medicine, Charlottesville, VA 22903; [n]Department of Microbiology, Immunology, and Cancer Biology, University of Virginia School of Medicine, Charlottesville, VA 22903; and [o]Department of Biomedical Engineering, University of Virginia School of Engineering, Charlottesville, VA 22904

Edited by Jeremy Nathans, Johns Hopkins University School of Medicine, Baltimore, MD, and approved December 19, 2019 (received for review July 8, 2019)

Degeneration of the retinal pigmented epithelium (RPE) and aberrant blood vessel growth in the eye are advanced-stage processes in blinding diseases such as age-related macular degeneration (AMD), which affect hundreds of millions of people worldwide. Loss of the RNase DICER1, an essential factor in micro-RNA biogenesis, is implicated in RPE atrophy. However, the functional implications of DICER1 loss in choroidal and retinal neovascularization are unknown. Here, we report that two independent hypomorphic mouse strains, as well as a separate model of postnatal RPE-specific DICER1 ablation, all presented with spontaneous RPE degeneration and choroidal and retinal neovascularization. DICER1 hypomorphic mice lacking critical inflammasome components or the innate immune adaptor MyD88 developed less severe RPE atrophy and pathological neovascularization. DICER1 abundance was also reduced in retinas of the JR5558 mouse model of spontaneous choroidal neovascularization. Finally, adenoassociated vector-mediated gene delivery of a truncated DICER1 variant (OptiDicer) reduced spontaneous choroidal neovascularization in JR5558 mice. Collectively, these findings significantly expand the repertoire of DICER1 in preserving retinal homeostasis by preventing both RPE degeneration and pathological neovascularization.

Dicer | retina | inflammasome | choroidal neovascularization

Age-related macular degeneration (AMD) is a prevalent disease affecting an estimated 1 in 40 persons worldwide (1). In its advanced, blinding stages, AMD manifests as progressive atrophy of retinal pigmented epithelium (RPE) and neuronal and vascular components of the choroid and retina. In contrast to atrophic AMD, wet or neovascular AMD is typified by the invasion of immature blood vessels into the outer retina from the retina and choroid. Although characterized by apparently distinct pathological processes, atrophic and neovascular AMD are overlapping conditions, with both forms of AMD observed in fellow eyes of an individual (2), within the same eye at sequential times, or even concurrently within the same eye (3).

Deficiency of DICER1, an RNase that processes double-stranded and self-complementary RNAs including a majority of premature micro-RNAs (miRNAs) into their bioactive forms (4–6), is among the inciting molecular events implicated in atrophic AMD (7–11). DICER1 also metabolizes transcripts from short interspersed nuclear element genetic repeats, principally *Alu* RNAs in humans and B1 and B2 RNAs in rodents (8, 9, 12–18). DICER1 deficiency is implicated in RPE cell death in atrophic AMD due to accumulation of unprocessed *Alu* RNAs, which results in noncanonical activation of the NLRP3 inflammasome, an innate immune pathway resulting in caspase-1–dependent maturation of IL-1β and IL-18 and RPE death (7–11, 19, 20).

Significance

DICER1 processes micro-RNAs into their bioactive forms and metabolizes RNAs from short interspersed nuclear element genetic repeats, principally *Alu* RNAs in humans. DICER1 deficiency is implicated in retinal pigmented epithelium (RPE) degeneration in atrophic age-related macular degeneration (AMD). Here, we report that three independent mouse models of DICER1 deficiency develop RPE degeneration and aberrant choroidal and retinal neovascularization (CRNV), both hallmarks of advanced AMD. These pathologies were dependent on inflammatory caspases 1 and 11 and the signaling adaptor MyD88. We observed reduced DICER1 abundance in a separate model of spontaneous CRNV and developed an adenoassociated vector-mediated DICER1 delivery construct, which reduced the severity of established spontaneous CRNV. Thus, persistent deficiency in DICER1 results in RPE degeneration and CRNV.

Author contributions: C.B.W., H.U., Y.K., T.Y., R.Y., S.H., R.D.M., I.A., F.P., Y.N., S.N., S.F., R.A., B.J.F., A.B.-C., N.K., B.K.A., J.A., and B.D.G. designed research; C.B.W., H.U., Y.K., T.Y., R.Y., S.H., R.D.M., I.A., F.P., Y.N., S.N., S.F., R.A., A.B.-C., B.K.A., and B.D.G. performed research; H.U., P.G., I.H., B.C., B.K.A., and B.D.G. contributed new reagents/analytic tools; C.B.W., H.U., Y.K., T.Y., R.Y., S.H., R.D.M., I.A., F.P., Y.N., S.N., S.F., R.A., B.J.F., A.B.-C., N.K., B.K.A., J.A., and B.D.G. analyzed data; and C.B.W., H.U., B.K.A., J.A., and B.D.G. wrote the paper.

Competing interest statement: J.A. is a co-founder of iVeena Holdings, iVeena Delivery Systems, and Inflammasome Therapeutics, and has been a consultant for Allergan, Biogen, Boehringer-Ingelheim, Immunovant, Janssen, Olix Pharmaceuticals, Retinal Solutions, and Saksin LifeSciences unrelated to this work. B.K.A. is a co-founder of iVeena Holdings, iVeena Delivery Systems, and Inflammasome Therapeutics, and has been a consultant to Alcon, Genentech, and Johnson & Johnson unrelated to this work. H.U., S.F., B.J.F., N.K., B.K.A., J.A., and B.D.G. are named as inventors on patent applications related to the intellectual property described in this manuscript that have been filed by the University of Virginia, the University of Kentucky, or the University of Utah.

This article is a PNAS Direct Submission.

[1]C.B.W. and H.U. contributed equally to this work.

[2]To whom correspondence may be addressed. Email: gelfand@virginia.edu.

[3]Present address: OliX Pharmaceuticals, Inc., Suwon-Si, Gyeonggi-do 16226, Korea.

[4]Present address: Vistar Eye Center, Roanoke, VA 24019.

This article contains supporting information online at https://www.pnas.org/lookup/suppl/doi:10.1073/pnas.1909761117/-/DCSupplemental.

First published January 21, 2020.

Conversely, the extent to which DICER1 activity affects vascular homeostasis of the choroid and outer retina is largely unknown. The outer retina is normally avascular, situated between the retinal and choroidal vascular networks. Maintenance of these strict vascular boundaries is essential for vision; anatomic disruption and exudation from aberrant neovessels into the outer retinal space are responsible for blindness in numerous ocular conditions, including neovascular AMD, pathologic myopia, polypoidal choroidal vasculopathy, and angioid streaks.

In this study, we investigated three different mouse models of DICER1 deficiency and performed restorative gene transfer in a separate model of spontaneous choroidal neovascularization, which collectively reveal that, in addition to promoting RPE atrophy, chronic DICER1 deficiency also stimulates pathological choroidal and retinal neovascularization (CRNV). These findings significantly expand the repertoire of DICER1 activities in maintaining choroidal and retinal vascular homeostasis in pathological processes that impair the vision of millions of individuals.

Results

Genetic Deficiency of Dicer1 Induces Spontaneous RPE Atrophy and Choroidal and Retinal Neovascularization in Three Independent Mouse Strains. Because loss of DICER1 is implicated in advanced atrophic AMD (7–11, 19, 21), we investigated whether chronic DICER1 deficiency in mice recapitulates retinal pathologies such as those observed in human AMD. Global ablation of *Dicer1* results in early embryonic lethality in mice (22, 23). Developmental or postnatal cell type-specific deletion of *Dicer1* in the RPE results in rapid and profound RPE and retinal atrophy (9, 24). In contrast, the *Dicer1*$^{Gt(\beta\text{-geo})Han}$ mouse line, hereafter referred to as *Dicer1*$^{d/d}$, harbors a gene trap insertion in intron 24 of the *Dicer1* locus, which results in a functional reduction in Dicer1 expression by ∼80% (25). The *Dicer1*$^{d/d}$ line is viable, with susceptibility to viral infections, exacerbated experimental rheumatoid arthritis, and infertility due to insufficient corpus luteal angiogenesis among its reported phenotypes (25–29). Consistent with its C57BL/6J background, *Dicer1*$^{d/d}$ did not exhibit hallmark features of the *rd8* mutation, a prevalent confounder of retinal phenotypes (30). DNA sequencing revealed that *Dicer1*$^{d/d}$ tested negative for the *rd8* mutation (*SI Appendix*, Fig. S1). Consistent with other tissues previously analyzed from this strain, retinal *Dicer1* mRNA abundance was reduced by ∼80% compared to wild-type littermate mice (*SI Appendix*, Fig. S2). As expected from prior studies on acute DICER1 deficiency in the RPE (7–11, 19, 21), *Dicer1*$^{d/d}$ mice exhibited spontaneous focal hypopigmented patches in fundus retinal images (Fig. 1*A*). Spectral domain optical coherence tomography (SD-OCT) revealed apically projected hyperreflective foci in the outer retina and RPE layers (Fig. 1*B*). The incidence of focal hypopigmentation of the fundus was age

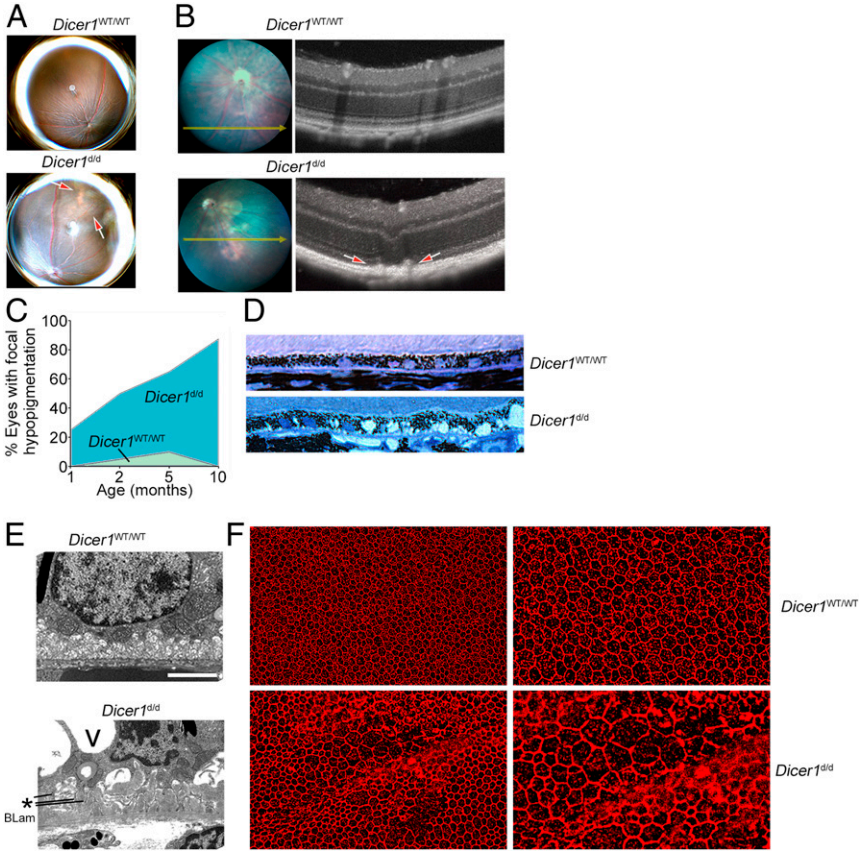

Fig. 1. (*A*) Representative fundus retinal photographs of age-matched 10-mo-old wild-type (WT) and *Dicer1*$^{d/d}$ mice. Note focal hypopigmentation present in *Dicer1*$^{d/d}$ eye denoted by red arrows. (*B*) Image-guided spectral-domain optical coherent tomography (SD-OCT) of a focal hypopigmented area of a WT (*Top*) and *Dicer1*$^{d/d}$ eye (*Bottom*). Note outer retinal discontinuity denoted by red arrows. (*C*) Incidence of focal hypopigmentation, tabulated as percentage of eyes, in WT and littermate *Dicer1*$^{d/d}$ with respect to age. $n = 48$ *Dicer1*$^{+/+}$ and 64 *Dicer1*$^{d/d}$ examinations were included in this analysis. Age was significantly associated with incidence of hypopigmentation by linear regression; $P = 0.0079$. (*D*) Toluidine blue-stained 1-μm-thick section of 15-mo-old *Dicer1*$^{d/d}$ (*Bottom*) demonstrates vacuolar, atrophied RPE layer compared to WT mice (*Top*). (*E*) Transmission electron micrograph of the basal aspect of RPE of 15-mo-old WT (*Top*) and *Dicer1*$^{d/d}$ (*Bottom*). RPE from *Dicer1*$^{d/d}$ mice exhibited large cytoplasmic vacuoles (V), loose basal infoldings (*), and debris at the interface of Bruch's membrane characteristic of basal laminar deposit (BLam). (Scale bar, 2 μm.) (*F*) Representative fluorescent micrographs of *Dicer1*$^{d/d}$ and WT littermate RPE flat mounts labeled with anti-Zonula Occludens-1 to label RPE tight junctions.

related, with 50% of eyes affected at 8 wk of age, and increased in frequency up to 75% at 10 mo of age ($P = 0.008$ by Spearman's rank coefficient test; Fig. 1*C*). Histological analysis revealed disorganized, hypertrophic RPE with large vacuoles (Fig. 1*D*). Ultrastructural analysis of *Dicer1*$^{d/d}$ retina revealed loose, disorganized RPE basal infoldings and extracellular sub-RPE debris consistent with basal laminar deposits (Fig. 1*E*), considered to be a general feature of distressed RPE that may have a role in AMD, but that is not specific for human AMD (31). Hypertrophy, disorganization, and RPE degeneration were also observed by flat-mount imaging of the RPE layer (Fig. 1*F*).

In addition, fluorescein angiography (FA) of *Dicer1*$^{d/d}$ mice revealed spontaneous hyperfluorescent foci that expanded over time, consistent with the behavior of immature vessels of active subretinal neovascular lesions (Fig. 2*A*). Conversely, no angiographically active lesions were observed in any eye from wild-type littermate at any age. SD-OCT of *Dicer1*$^{d/d}$ mice revealed outer retinal discontinuities consistent with choroidal neovascularization (Fig. 2*B*). The incidence and severity of FA-positive lesions were quantified using an established grading scale (32, 33). Both lesion incidence and severity were significantly associated with age ($P < 0.001$ by Spearman's rank coefficient test; Fig. 2*C*). In the majority of *Dicer1*$^{d/d}$ mouse eyes harboring angiogenic lesions, most exhibited one discrete lesion, but occasionally more than one lesion was present. Histological examination revealed type 1 (sub-RPE) (Fig. 2*D*) and type 2 (subretinal) choroidal neovascular (CNV) lesions and type 3 chorioretinal anastomoses in the outer retina (*SI Appendix*, Fig. S3). Vessels were patent with erythrocytes observed surrounded by an intimal layer of endothelial cells. Choroidal endothelial cells were observed traversing Bruch's membrane (*SI Appendix*, Fig. S4). These findings are consistent with CNV in humans and in other experimental models. Administration of a Vegfa-neutralizing antibody (B20-4.1.1) into the vitreous humor reduced the angiographic activity of neovascular lesions (Fig. 2*E*), suggesting that neovascularization due to Dicer1 deficiency recapitulates the therapeutic response to anti-VEGFA compounds observed in aberrant neovascularization in human patients.

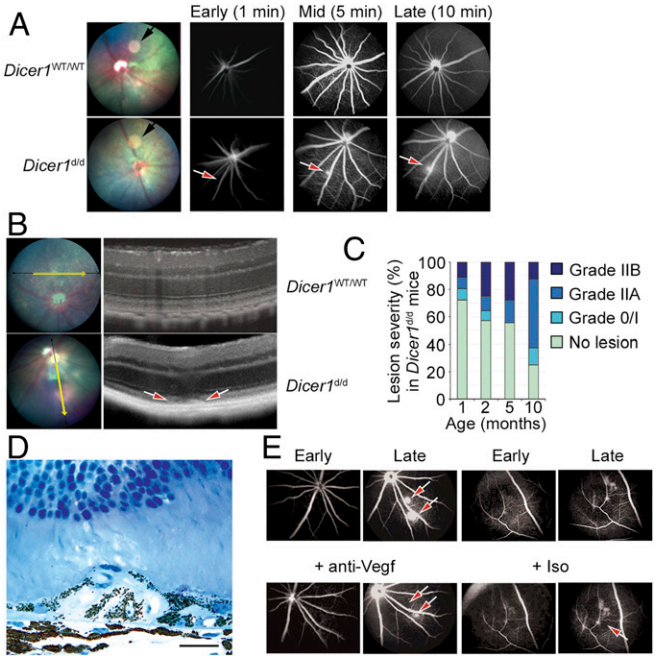

Fig. 2. (*A*) Fundus retinal imaging (*Left*) and early, mid, and late fluorescein angiograms of wild-type (WT) littermate and *Dicer1*$^{d/d}$ mice. The black arrow in fundus retinal image denotes circular image artifact. The red arrow denotes focal hyperfluorescent neovascular lesion. (*B*) Image-guided SD-OCT of a WT littermate (*Top*) and *Dicer1*$^{d/d}$ mouse eye (*Bottom*). The red arrows denote neovascular lesion. (*C*) Incidence and severity of neovascular lesions *Dicer1*$^{d/d}$ with respect to age. Ninety individual examinations were included in this analysis. No vascular lesions were detected in WT littermate mice at any age. Age was significantly associated with incidence and severity of neovascular lesions by linear regression ($P = 0.0184$) and Spearman's rank ($P < 0.00058$), respectively. (*D*) High-magnification toluidine blue-stained 1-μm-thick section of a neovascular lesion in a 12-mo-old *Dicer1*$^{d/d}$ mouse shows RPE delamination and migration. Scale bar, 20 microns. (*E*) Representative early and late fluorescein angiograms of *Dicer1*$^{d/d}$ mouse prior to and 3 d after intravitreous injection of Vegf neutralizing antibody or isotype. The red arrows denote neovascular lesion that resolved following Vegf neutralization.

To more thoroughly evaluate the effect of genetic inhibition of Dicer1 on atrophic and neovascular retinal pathologies, we investigated a second Dicer1 hypomorphic mouse strain, *Dicer1*$^{Gt(RRF266)Byg}$ (hereafter *Dicer1*$^{H/H}$), generated by a different laboratory by inserting a gene trap vector into a different region (intron 22) of the *Dicer1* locus and maintained on a different genetic background (34, 35). Dicer1 abundance in the retina of *Dicer1*$^{H/H}$ mice was ∼65% less than their wild-type littermate controls (*SI Appendix*, Fig. S5). *Dicer1*$^{H/H}$ mice also exhibited spontaneous RPE degeneration, as evidenced by focal hypopigmentation on fundus photography (Fig. 3*A*) and foci of active neovascular lesions by FA (Fig. 3*B*), which localized to the subretinal space upon imaging with SD-OCT (Fig. 3*C*). Histological analysis revealed focal RPE thinning and choroidal neovascularization (Fig. 3 *D*–*G*). Aberrant angiogenic lesions were absent in littermate controls; angiographic leakage was detected in 0 of eight eyes *Dicer1*$^{wt/wt}$ vs. six of eight eyes *Dicer1*$^{H/H}$ ($P = 0.003$ by Fisher's exact test). Thus, two independent mouse models of systemic DICER1 deficiency, developed by different laboratories, targeting distinct regions of the *Dicer1* locus, and maintained on different genetic backgrounds both exhibit spontaneous RPE atrophy and choroidal neovascularization.

Given that Dicer1 ablation in the RPE can promote RPE atrophy (9, 24), we sought to determine whether loss of Dicer1 in the RPE was likewise sufficient to promote neovascularization. Enforced Dicer1 ablation in RPE was accomplished by subretinal injection of an adenoassociated virus (AAV) that encoded codon-optimized Cre recombinase (iCre) under the control of an RPE-specific promoter (0.8 kb of the human RPE65 promoter) [AAV2-hRPE(0.8)-iCre-WPRE; Vector Biolabs] into *Dicer1*$^{flox/flox}$ mice (36). As in prior studies (9), we observed RPE degeneration in nine of nine AAV-Cre-treated eyes by fundus photography and SD-OCT within 10 d of AAV treatment, consistent with the latency of Cre expression in this system. Within 24 d of AAV administration, we found evidence of active choroidal neovessels by FA and SD-OCT in six of nine treated eyes, compared to 0 of four AAV-Cre–treated wild-type eyes ($P = 0.043$, log-rank test; Fig. 4 *A*–*C*). We confirmed the choroidal origin of these neovessels by immunofluorescent histology (Fig. 4*D*). We interpret these findings to indicate that Dicer1 deficiency in RPE is sufficient to promote CNV in mice.

Collectively, findings from three models of Dicer1 deficiency indicate that, in addition to maintaining RPE integrity, Dicer1 plays a critical role in maintaining outer retinal avascularity.

RPE Degeneration and Aberrant Angiogenesis due to DICER1 Loss Depends on Innate Immune Signaling. Acute DICER1 antagonism in the RPE promotes activation of the inflammasome, leading to RPE degeneration (11). We sought to determine the extent to which inflammasome contributes to RPE atrophy and CNV due to chronic DICER1 deficiency. We first investigated inflammasome activity in *Dicer1*$^{d/d}$ mice. Transcripts encoding the NLRP3 inflammasome-related genes *Casp1* and *Nlrp3*, and the effector cytokine *Il18* were up-regulated in retinas of *Dicer1*$^{d/d}$ mice compared to littermate controls (*SI Appendix*, Fig. S6).

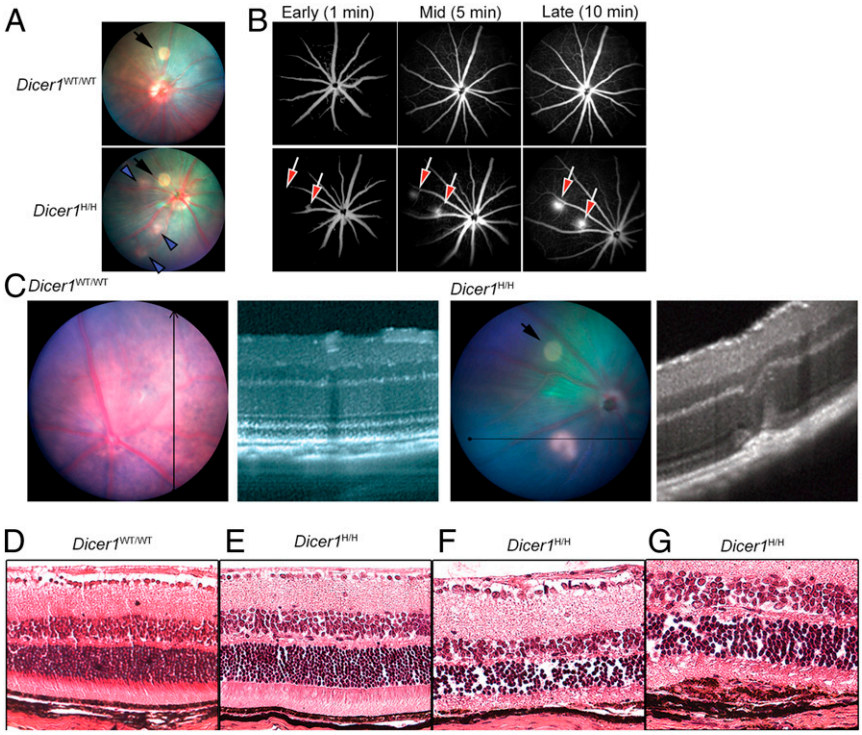

Fig. 3. (*A*) Representative fundus retinal photograph of *Dicer1*$^{H/H}$ and littermate control. The black arrows denote camera artifact. The blue arrowheads denote patches of focal hypopigmentation. (*B*) Representative early, middle, and late fluorescein angiograms show active areas of neovascularization in *Dicer1*$^{H/H}$ eyes. No fluorescein leakage was detected in littermate wild-type (WT) eyes. (*C*) Image-guided SD-OCT image of normal littermate WT eye (*Left*) and a neovascular lesion in a *Dicer1*$^{H/H}$ mouse showing disruption of outer retinal architecture (*Right*). The black arrow in fundus retinal image denotes circular image artifact. (*D*–*G*) Hematoxylin and eosin-stained sections from WT littermate and *Dicer1*$^{H/H}$ eyes. Whereas WT (*D*) and areas of *Dicer1*$^{H/H}$ (*E*) appear anatomically normal, focal areas of *Dicer1*$^{H/H}$ mice exhibited RPE atrophy (*F*) and subretinal neovascular membranes (*G*).

Inflammasome activation, measured by in situ proteolytic activity of a fluorescent Caspase-1 peptide substrate, was also observed in the outer retinae of *Dicer1*$^{d/d}$ mice in areas of neovascularization (*SI Appendix*, Fig. S7).

We next sought to ascertain the relationship between DICER1 deficiency and immune signaling constituents in promoting spontaneous retinal pathologies. Dicer1-deficient mice lacking the inflammatory effector caspases 1 and 11 (*Dicer1*$^{d/d}$; *Casp1*$^{-/-}$; *Casp11*$^{-/-}$) exhibited a significantly reduced incidence of focal hypopigmentation compared to caspase-1 and -11 sufficient *Dicer1*$^{d/d}$ mice ($P < 0.001$ by multinomial logistic regression; Fig. 5*A*). Ablation of caspases 1 and 11 also reduced the incidence and severity of pathological neovascular lesions by FA grading ($P < 0.001$; Fig. 5 *B* and *C*). The adaptor MyD88, a putative drug target for AMD (11), transduces several inflammatory stimuli emanating from Toll-like receptors (TLRs) (excluding TLR3) and receptors for inflammasome effector cytokines IL-1β and IL-18. Dicer1-deficient mice lacking MyD88 (*Dicer1*$^{d/d}$; *Myd88*$^{-/-}$) also exhibited significantly reduced incidence of focal RPE hypopigmentation ($P < 0.001$; Fig. 5*A*) and incidence and severity of pathological neovascular lesions ($P < 0.001$; Fig. 5*C*). Together, we interpret these findings to indicate that signaling through caspases 1 and 11 and MyD88 mediate both atrophic and neovascular retinal pathologies that arise due to chronic DICER1 deficiency.

DICER1 Dysregulation in Spontaneous CNV JR5558 Mice. Given the findings that Dicer1 deficiency in mice promotes spontaneous neovascularization, we sought to quantify the expression of DICER1 in the JR5558 mouse line, which develops spontaneous CNV (37, 38) that is dependent on the *rd8* mutation in the Crb1 gene locus (39). Similar to CNV in humans and in Dicer1-deficient mice, neovascular lesions in JR5558 also respond to VEGF neutralization (38, 40) and depend on innate immune processes (38, 41, 42). Compared to age-matched wild-type mice, Dicer1 abundance was significantly reduced in the RPE of JR5558 mice at postnatal days 9–10 (P9–P10), coincident with the earliest reported neovascular abnormalities, and reduced DICER1 levels persisted to P28–P37 (Fig. 6*A* and *SI Appendix*, Fig. S8). Conversely, Dicer1 abundance in neural retina was elevated compared to age-matched wild-type controls when measured in P9–P10 and reduced at P28–P37 (Fig. 6*B*). Thus, Dicer1 dysregulation is coincident with the earliest stages of neovascular defects in JR5558 mice, and Dicer1 deficiency in RPE precedes loss in neural retina at later time points. We interpret these data to indicate that Dicer1 expression is dysregulated in spontaneous CNV of mice.

Development of the OptiDicer Construct. To determine the functional contribution of Dicer1 deficiency to retinal and choroidal neovascularization in JR5558 mice, we developed a gene therapy capable of restoring Dicer1 activity. We selected adenoassociated vector (AAV) because this modality has demonstrated safety and efficacy in treating blinding diseases in human patients (43, 44) and in experimental models of CRNV (45–50). The human and mouse DICER1 genes are encoded by sequences of 5.7 kb, which is too large to be packaged into a traditional AAV with a size limit of ∼5.2 kb (51, 52). The large N-terminal helicase domain of DICER1 is known to be dispensable for miRNA substrate specificity and processing activity (53–55). In a tube assay, we confirmed that purified helicase domain-deleted human DICER1 (Δhel-DICER1) retained pre-miRNA processing activity, and that purified human DICER1 lacking the PAZ domain necessary for pre-miRNA recognition (ΔPAZ-DICER1)

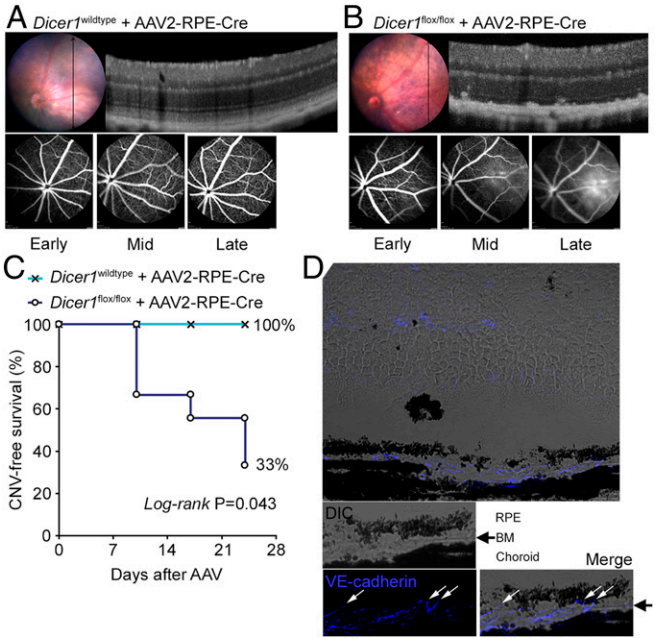

Fig. 4. (*A*) Image-guided SD-OCT image and FA of a wild-type eye 24 d after subretinal injection with AAV encoding RPE-specific Cre recombinase. Representative of $n = 4$ eyes. (*B*) Image-guided SD-OCT image and FA of a *Dicer1*$^{flox/flox}$ eye 24 d after subretinal injection with AAV encoding RPE-specific Cre recombinase. (*C*) Kaplan–Meier plot of CNV-free survival in AAV-treated *Dicer1*$^{wild\text{-}type}$ and *Dicer1*$^{flox/flox}$ eyes. By 24 d after AAV administration, RPE degeneration was observed in 100% (nine of nine) eyes of *Dicer1*$^{flox/flox}$ mice and active neovascular lesions were detected in 67% (six of nine) eyes. (*D*) Histopathology of AAV-treated *Dicer1*$^{flox/flox}$ eye demonstrating choroidal vessels traversing Bruch's membrane (BM). The white arrows denote VE-cadherin–positive (pseudo-colored blue) endothelial cell crossing BM (black arrow).

(56, 57) did not (Fig. 7*A* and *SI Appendix*, Fig. S9). The coding sequence of Δhel-DICER1 is 3.9 kb, which is compatible with efficient AAV packaging. Δhel-DICER1 cDNA was cloned into pAAV-MCS, with a total packaging genome size, including regulatory elements and AAV inverted terminal repeats, of 5.0 kb.

Transient transfection of Δhel-DICER1 resulted in robust expression in HeLa cells as detected by immunoblotting (Fig. 7*B*). However, transfection into human RPE cells resulted in no detectable expression of the truncated protein. Therefore, we hypothesized that DICER1 expression in RPE was subject to negative autoregulation, potentially arising due to the enhanced miRNA processing activity of DICER1. Consistent with this hypothesis, transient Δhel-DICER1 expression was observed within 4 h of transfection, but reduced to undetectable levels soon thereafter (Fig. 7*C*). Furthermore, cotransfection with double-stranded RNA, which can compete with DICER1 processing and RISC loading (58), restored Δhel-DICER1 expression to detectable levels (Fig. 7*D*). We interpret these results to indicate that impaired Δhel-DICER1 expression was due to negative feedback via RNA interference.

Because the Δhel-DICER1 insert lacks a native 3′-untranslated region, we hypothesized that miRNA binding sites within the coding sequence were responsible for negative feedback. Forman et al. (59) demonstrated that let-7 miRNAs specifically target the DICER1 coding region, identifying three putative target regions. Based on this study, we generated let-7–resistant Δhel-DICER1 with silent mutations of these three targets. Although let-7–resistant Δhel-DICER1 was robustly expressed in HeLa cells, it too failed to express in human RPE cells in detectable levels (Fig. 7*E*). Therefore, we next sought to generate a pan-miRNA–resistant Δhel-DICER1. We utilized miRDB (http://mirdb.org/miRDB/index.html) (60, 61), which identified 44 miRNA seed sequences (37 human and 7 mouse) within the Δhel-DICER1 coding region. We successfully removed 33 of these putative seed sequences (28 human and 5 mouse) by introducing silent mutations. The resulting construct, OptiDicer, exhibited robust and stable expression in human RPE cells (Fig. 7*E*).

Gene Delivery of OptiDicer Improves Spontaneous Chorioretinal Neovascularization in Mice. Stable expression of AAV-encoded OptiDicer was confirmed in retina of JR5558 mice by immunoblotting and in situ hybridization achieved by probes recognizing OptiDicer sequence (Fig. 8 *A* and *B*). Consistent with the established tropism of AAV serotype 2 (62, 63), transgene expression was localized to multiple outer retinal cell types, including RPE (Fig. 8*B*). To determine whether DICER1 gene delivery affected CRNV in JR5558 mice, first, FA was performed on naive 6-wk-old JR5558 mice with established CNV. Then, AAV-OptiDicer or an empty AAV2-control was administered by subretinal injection in contralateral eyes. Fourteen and 28 d after injections, follow-up FA revealed significant improvement in both the frequency and severity of neovascular lesions within injected areas compared to eyes transduced with a control vector (Fig. 8 *C* and *D*). Together, we interpret these studies to suggest that subretinal delivery of a bioactive DICER1 variant by AAV antagonizes CRNV in JR5558 mice.

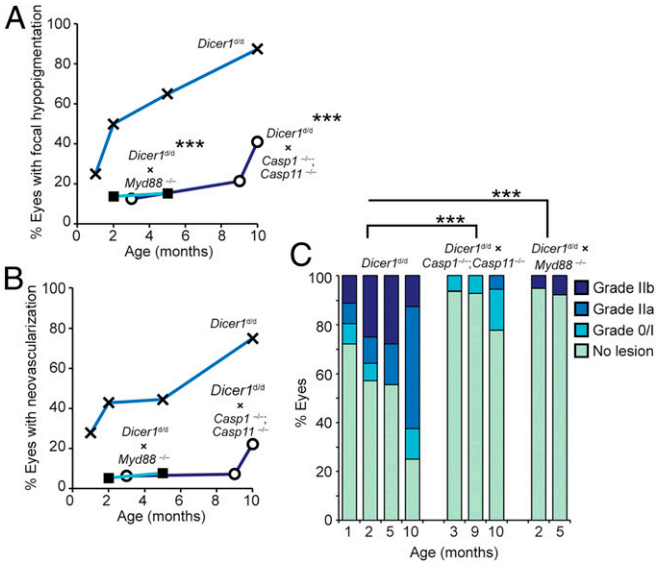

Fig. 5. (*A*) Analysis of the incidence of focal hypopigmentation with respect to age in *Dicer1*$^{d/d}$ ($n = 64$ examinations), *Dicer1*$^{d/d}$; *Casp1*$^{-/-}$; *Casp11*$^{-/-}$ ($n = 47$), and *Dicer1*$^{d/d}$; *Myd88*$^{-/-}$ ($n = 62$). The effect of genotype on the presence of focal hypopigmentation was quantified by nominal regression using genotype and age as dependent variables and the presence or absence of focal hypopigmentation as an independent variable. Ablation of *Casp1*/ *Casp11* and *Myd88* were associated with significantly reduced hypopigmentation; ***$P < 0.001$. (*B* and *C*) Angiogram grading of *Dicer1*$^{d/d}$ ($n = 91$), *Dicer1*$^{d/d}$; *Casp1*$^{-/-}$; *Casp11*$^{-/-}$ ($n = 48$), and *Dicer1*$^{d/d}$; *Myd88*$^{-/-}$ ($n = 64$). (*B*) Incidence of vascular lesion-positive eyes with respect to age. (*C*) Severity of neovascular lesions with respect to age. The effect of genotype on the severity of neovascular lesions was quantified by nominal regression using genotype and age as dependent variables and the neovascular lesion grade as an independent variable. Ablation of *Casp1*/ *Casp11* and *Myd88* were associated with significantly reduced neovascular severity; ***$P < 0.001$.

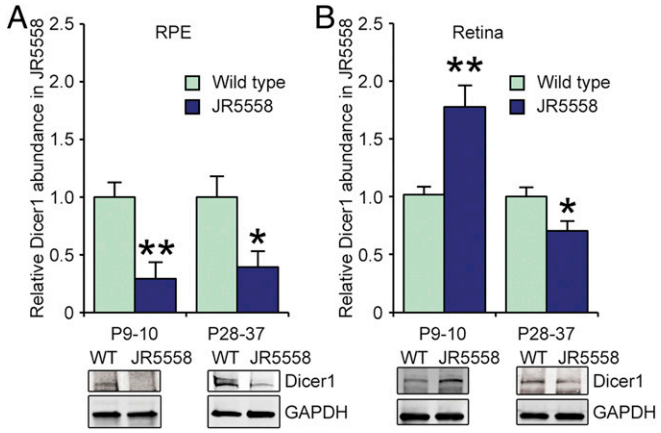

Fig. 6. Densitometry of Dicer1 abundance by immunoblotting of RPE (*A*) and retina (*B*) from WT and JR5558 mice of indicated ages. $n = 5–11$. Dicer1 levels were normalized to GAPDH. $*P < 0.05$, $**P < 0.01$ compared to WT Dicer1 levels.

Discussion

We report that genetic suppression of Dicer1 in three independent mouse models manifests in the eye as focal RPE atrophy and aberrant CRNV, and that DICER1 expression is reduced in a mouse model of spontaneous CNV. Furthermore, we report that AAV-enforced expression of a DICER1 construct, which successfully escaped miRNA negative feedback, reduces spontaneous CNV in mice. In addition to expanding upon prior studies of DICER1 loss in atrophic AMD, these findings identify maintenance of outer retinal avascularity as another critical function of DICER1 in maintaining retinal homeostasis.

One limitation of the current study is that one cannot conclude whether neovascularization in Dicer1-deficient mice is an independent, pleiotropic effect of Dicer1 deficiency, or whether it is secondary to the RPE changes that develop with age in this strain. Importantly, CRNV lesions occur in Dicer1-deficient mice in the absence of frank RPE degeneration (Fig. 2*D* and *SI Appendix*, Fig. S3) and in JR5558 mice in which DICER1 expression is reduced. Additionally, sodium iodate administration, a well-characterized model of RPE death (64, 65), is not reported to promote spontaneous neovascularization. Thus, CRNV is not a generic response secondary to RPE death, and if CRNV arises due to secondary effects of RPE changes, it is likely due to RPE damage that occurs in a Dicer1-specific manner.

Similar to organism-wide hypomorphic strains, Dicer1 ablation in RPE specifically resulted in neovascularization. Although these findings suggest that Dicer1 deficiency in RPE is sufficient to drive neovascularization, the role of Dicer1 deficiency in cells other than RPE on neovascularization cannot be excluded. Important similarities of these models include the insult of Dicer1 deficiency, although the degree and cell type specificity differ. The phenotypes of RPE atrophy and CNV occur in all three models. Key differences among these models include that, compared to the hypomorphic strains, the RPE ablation model develops relatively large, diffuse vascular lesions that colocalize to areas of profound RPE defects. They also differ in kinetics of pathologies, wherein the *Dicer1*$^{d/d}$ strain develops outer retinal pathologies over months compared to weeks in the ablation model. These differences may arise as a consequence of the different degrees of Dicer1 insufficiency (hypomorphic expression vs. knockout) or cell type-specific effects of Dicer1 loss.

The established role of DICER1 in mediating developmental and pathological angiogenesis and neovascularization is largely context- and tissue type-dependent. For example, whereas DICER1 ablation prevents developmental and postnatal angiogenesis in multiple diverse settings (23, 66–69), DICER1 deficiency can promote neovascularization in stroke (70), angiosarcoma (71), and renal cell carcinoma (72, 73). Furthermore, exogenous delivery of DICER1 suppresses tumor angiogenesis (72) and hypoxia-induced angiogenic responses in human endothelial cells (74). The present findings suggest that, in the outer retina, DICER1 expression serves to prevent pathological neovascularization.

The downstream effects of DICER1 down-regulation, including modulation of angiogenesis, have most commonly been attributed to loss of miRNA biogenesis. It will be important in future work to establish whether miRNA or noncanonical DICER1 substrates such as *Alu* RNAs, which promote RPE degeneration due to DICER1 loss, also contribute to neovascular and degenerative phenotypes observed in this study.

Because of the unique features of the *Dicer1*$^{d/d}$ mouse line, including exhibiting multiple AMD-related pathologies such as DICER1 deficiency, inflammasome activation and dependence, relatively early onset of phenotypes, age dependence of pathological incidence and severity, and facile phenotypic scoring, this model may be of interest to both basic discovery and translational research as a preclinical testing platform. Unlike other more acute and severe models of CRNV such as the JR5558 and *Vldr*$^{-/-}$ lines, the pathologies in Dicer1 hypomorphic mice are less severe and incompletely penetrant at the ages reported. This suggests that Dicer1 deficiency may promote an environment wherein development of CRNV is stochastic with a threshold that diminishes over time. Additionally, the outer retina may possess compensatory mechanisms to abate the development of pathologies due to DICER1 deficiency that are gradually lost with age. The penetrance in Dicer1 hypomorphic mice is greater

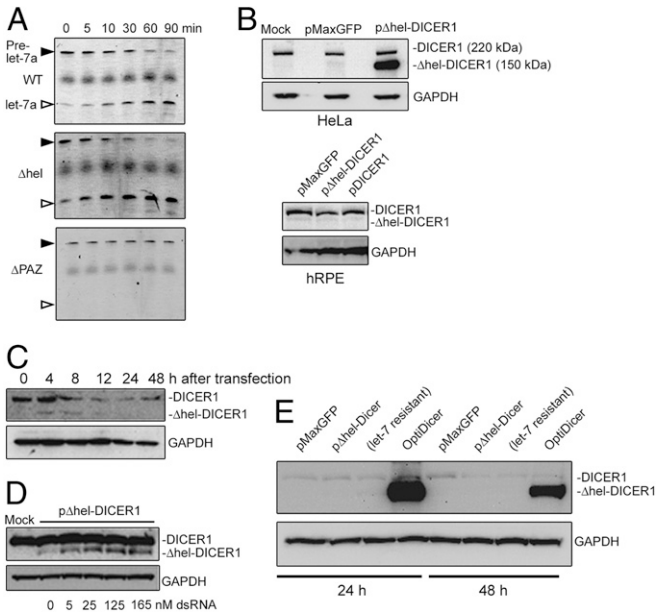

Fig. 7. (*A*) In vitro processing assay of pre-miRNA of DICER1, Δhel-DICER1, and ΔPAZ-DICER1 purified from HEK 293T cells. (*B*) Immunoblotting of HeLa and primary human RPE (hRPE) after transient transfection with plasmids to express GFP (pMaxGFP), Δhel-DICER1 (pΔhel-DICER1), or full-length human DICER1 (pDICER1). (*C*) Time course of Δhel-DICER1 expression in hRPE cells after transient transfection. Note faint detection of Δhel-DICER1 at 4 and 8 h after transfection. (*D*) Dose-dependent effect of dsRNA cotransfection on Δhel-DICER1 in hRPE. (*E*) Expression of endogenous and Δhel-DICER1 in primary hRPE 24 and 48 h after transfection with indicated DICER1 constructs.

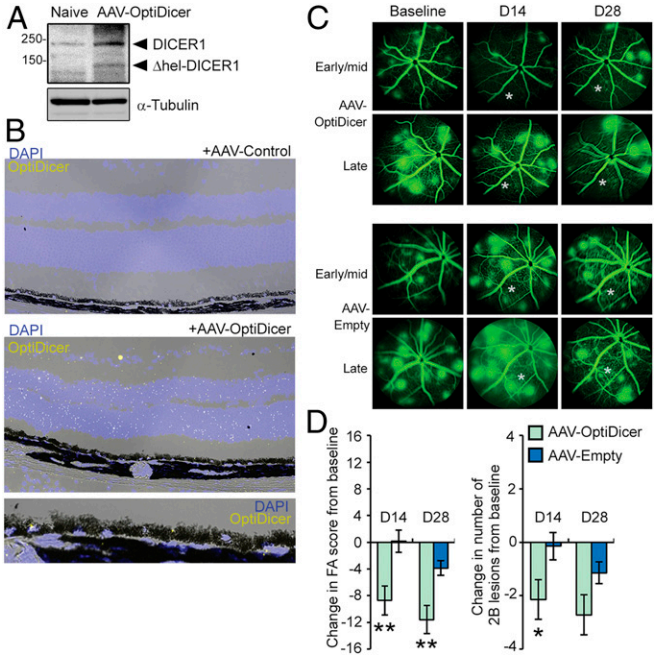

Fig. 8. Detection of Δhel-DICER1 in retina following subretinal injection of AAV-OptiDicer by immunoblotting (*A*) and in situ hybridization using a probe antisense to the synthetic OptiDicer sequence (*B*). (*C*) Representative fluorescein angiograms of JR5558 mice prior to, and 14 and 28 d after subretinal injection of AAV-OptiDicer or AAV-Empty. Injections were made in an area encompassing the lower left quadrant of the fundus relative to the optic nerve. Approximate injection site is denoted by an asterisk (*). (*D*) Quantification of changes in total FA score and number of 2B lesions from baseline after AAV-OptiDicer- and AAV-Empty-injected eyes ($n = 7$ eyes/treatment). $^*P < 0.05$; $^{**}P < 0.01$.

than other models of CRNV such as the *Sod1*$^{-/-}$ (75), and *Ccr2*$^{-/-}$ and *Ccl2*$^{-/-}$ strains (76).

This study also suggests that restoring DICER1 expression in the retina could itself be a viable therapeutic target in physiologic and pathologic conditions. Of note, the efficacious DICER1 gene delivery does not necessarily implicate DICER1 deficiency as a proximal cause of neovascularization in JR5558 mice. For example, it is possible that restoring DICER1 levels enhances activity of a beneficial miRNA through improved miRNA processing, although its inefficient processing due to DICER1 reduction was not a proximal cause of the neovascularization. Identifying the precise molecular mechanisms by which DICER1 gene therapy affects retinal phenotypes is an important avenue of future research.

Materials and Methods

Mice. All experiments involving animals were approved by the University of Virginia Animal Care and Use Committee and in accordance with the Association for Research in Vision and Ophthalmology Statement for the Use of Animals in Ophthalmic and Visual Research. Mice were maintained on a constant 12:12-h light–dark cycle. Water and food were provided ad libitum. Mice were euthanized with CO_2 gas under constant gas flow. C57BL/6J wild-type mice were obtained from The Jackson Laboratory. The *Dicer1*$^{d/d}$ mouse strain backcrossed to C57BL/6J and the *Dicer1*$^{H/H}$ were maintained in a heterozygous state, and homozygous wild-type and mutant littermates were utilized for experiments. The *Dicer1*$^{d/d}$ strain was bred to *Myd88*$^{-/-}$ (The Jackson Laboratory) and *Casp1*$^{-/-}$/*Casp11*$^{-/-}$ (77), a generous gift from Gabriel Nuñez (University of Michigan, Ann Arbor, MI). *Dicer1*$^{flox/flox}$ were obtained from the Jackson Laboratory (JAX stock #006366). JR5558 mice (The Jackson Laboratory) were maintained as previously described (37, 38).

Retinal Imaging and Angiography. Retinal photographs of dilated mouse eyes were taken with a TRC-50 IX camera (Topcon) linked to a digital imaging system (Sony) or with the Mm IV Retinal Microscope (Phoenix Research Labs). SD-OCT was acquired with an OCT2 scan head attached to a Mm IV Retinal Microscope (Phoenix). Fluorescein angiograms were used to measure the incidence and severity of CRNV. In anesthetized mice with dilated eyes, sodium fluorescein (0.1 mL of 2.5% solution) was injected into the peritoneum, and then eyes were imaged with a fluorescent microscopic camera (TTRC-50IX, Topcon; or Mm IV, Phoenix) for up to 10 min to monitor dye leakage. Images were graded by a trained operator blinded to the treatment groups. For AAV treatment study, the parameter "FA score" was developed to capture both the number and severity of angiographically active lesions. Lesions were only counted in the area corresponding to the injected site, determined anatomically. For each eye, FA score was calculated as follows:

$$\text{FA Score} = n_{\text{Grade 0 lesions}} + 2^* n_{\text{Grade 1 lesions}} + 3^* n_{\text{Grade 2a lesions}} + 4^* n_{\text{Grade 2b lesions}}.$$

Histology, Immunohistochemistry, Immunofluorescence, and in Situ Hybridization. For hematoxylin and eosin staining and immunofluorescence, fresh, unfixed mouse eyes were embedded in Optimal Cutting Temperature Compound (Fisher), frozen in isopentane precooled by liquid nitrogen, and cryosectioned at 10 μm. Immunofluorescent staining was performed with a goat antibody against VE-cadherin (1:50; Santa Cruz). Bound antibody was detected with anti-goat secondary antibody (Thermo Fisher). For detection of OptiDicer mRNA, in situ hybridization was performed using RNAscope (ACD Biosciences) according to manufacturer's instructions.

RNA Isolation and Real-Time Quantitative PCR Analysis. Tissue was collected and homogenized in TRIZOL (Thermo Fisher) following the manufacturer's protocol. Total RNA was DNase treated and reverse transcribed using QuantiTect Reverse Transcription Kit (Qiagen). The RT products (cDNA) were amplified by real-time quantitative PCR (Applied Biosystems 7900 HT Fast Real-Time PCR system) with Power SYBR green Master Mix. Oligonucleotide primers specific for mouse *Casp1* (forward, 5′-ACC CTC AAG TTT TGC CCT TT-3′, and reverse, 5′-GAT CCT CCA GCA GCA ACT TC-3′), *Il1b* (forward, 5′-GGG CCT CAA AGG AAA GAA TC-3′, and reverse, 5′-TAC CAG TTG GGG AAC TCT GC-3′), *Il18* (forward, 5′-GAC AGC CTG TGT TCG AGG AT-3′, and reverse, 5′-TGG ATC CAT TTC CTC AAA GG-3′), *Nlrp3* (forward, 5′-ATG CTG CTT CGA CAT CTC CT-3′, and reverse, 5′-AAC CAA TGC GAG ATC CTG AC), and 18S rRNA (forward, 5′- TTCGTATTGCGCCGCTAGA-3′, and reverse, 5′- CTTTCG-CTCTGGTCCGTCTT-3′) were used. Oligonucleotide primers spanning exons 24 and 25 to detect *Dicer1* abundance in *Dicer1*$^{d/d}$ mice were utilized as previously described (25).

The qPCR cycling conditions were 50 °C for 2 min, 95 °C for 10 min, followed by 40 cycles of a two-step amplification program (95 °C for 15 s and 58 °C for 1 min). At the end of the amplification, melting curve analysis was applied to exclude contamination with unspecific PCR products. Relative expressions of target genes were determined by the $2^{\Delta\Delta Ct}$ method.

Western Blotting. Purified retina and RPE protein lysates were obtained using an established protocol (78). For RPE, eyes from three to five eyes were pooled, constituting one independent observation. Purified RPE isolation was confirmed by the presence of the RPE-specific marker RPE65 and absence of the rod photoreceptor protein Rhodopsin by immunoblotting. Protein concentrations were determined using a bicinchoninic acid assay kit (Thermo Fisher) with BSA as a standard. Proteins (40 to 100 μg) were run on Tris-glycine gels (Invitrogen or Bio-Rad) and transferred to PVDF membranes. The transferred membranes were blocked for 1 h at room temperature (RT) and incubated with antibodies against human and mouse DICER1 (Bethyl; 1:500), RPE65 (Novus; 401.8B11.3D9; 1:1,000), VE-cadherin (Santa Cruz; C-19; 1:250), Rhodopsin (Abcam; 1D4; ab5417; 1:1,000), GAPDH (Abcam; ab83956; 1:1,000), β-Actin (Abcam; ab8229; 1:1,000), and α-Tubulin (Abcam; ab89984; 1:1,000). IRdye-conjugated secondary antibodies were used (1:5,000) for 1 h at RT. The signal was visualized by Licor Odyssey and densitometry quantified by ImageJ.

In Situ Caspase-1 Activity. In situ detection of Caspase-1 activity was conducted as described previously (8). Briefly, unfixed eyes were enucleated and immediately placed in OCT mounting media and snap frozen in isopentane cooled by liquid nitrogen. Unfixed 5-μm-thick frozen sections of mouse eyes were incubated with CaspaLux1-E1D2 (Oncoimmunin) for 40 min at 37 °C in a humidified chamber. Afterward, slides were washed five times in PBS. Coverslips were placed on the tissue sections, and fluorescent and bright-field images were acquired on a Nikon Eclipse Ti inverted fluorescent microscope.

miRNA Preparation. The 5′ and 3′ prelet-7a miRNA constructs were synthesized by Integrated DNA Technologies. Annealing and ligation protocols were adapted from ref. 79. Briefly, a 20-μL mixture containing 200 pmol of 5′ strand and 100 pmol of 3′ strand in TE buffer with 100 mM NaCl was annealed by heating to 95 °C, and then slowly cooling (−1 °C per 30 s) to 25 °C. Subsequent ligation was achieved by incubating the annealed substrate with 3 μL of T4 RNA ligase (Ambion; 5 U/μL), 3 μL of 0.1% BSA, 5 μL of 10× ligation buffer, and 19 μL of ultrapure water at 16 °C for 24 h. RNA was isolated by standard ethanol precipitation and resuspended in 10 μL of 2× TBE-urea loading dye (Bio-Rad) and 10 μL ultrapure water. After separation on a Novex 15% TBE-urea gel (Thermo Fisher Scientific), the gel was incubated in GelStar Nucleic Acid Gel Stain 10,000× (Lonza) and visualized on a UVP High Performance UV Transilluminator (AnalytikJena). Ligated miRNA was excised from the gel, crushed in a 1.5-mL Eppendorf tube, and incubated in 200 μL of 0.3 M NaCl-TE (pH 7.5) overnight. Crushed gel solution was filtered through an EDGE DTR filter column (EdgeBio) and precipitated via standard ethanol precipitation. 5′ sequence was as follows: 5′-UGA GGU AGU AGG UUG UAU AGU UUU AGG GUC ACA CC-3′; 3′ sequence was as follows: 5′-pCAC CAC UGG GAG AUA ACU AUA CAA UCU ACU GUC *Cy5*UU CU-3′.

In Vitro DICER1 Tube Assay. DICER1 plasmids were transfected into HEK293T cells with Lipofectamine 2000 (Thermo Fisher Scientific) according to the manufacturer's protocol. Protein was collected after 48 h as in ref. 80. Briefly, cells were collected in 1 mL of lysis buffer (500 mM NaCl, 1 mM EDTA, 20 mM Tris [pH 8.0], 1% Triton X-100) and incubated on ice for 20 min. After sonication, cells were centrifuged twice at 16,000 × *g* for 10 min, and supernatant was transferred to 1.5-mL Eppendorf tube. One hundred microliters of anti-FLAG M2 magnetic beads were equilibrated according to the manufacturer's protocol and incubated with protein supernatant overnight on an end-to-end tube rotator at 4 °C. Beads were washed three times with lysis buffer and four times with Buffer D (200 mM KCl, 20 mM Tris [pH 8.0], 0.2 mM EDTA). The FLAG-DICER1 was eluted from the beads by competition with 250 μL of FLAG peptide (100 μg/mL; Sigma-Aldrich). To remove excess FLAG peptide, eluate from the competition was passed through an Amicon 100-kDa cutoff filter (Millipore Sigma).

In vitro DICER1 cleavage assay was adapted from ref. 80. Briefly, reactions were performed in a total volume of 10 μL containing 1 μL of 10× DICER reaction buffer (100 mM Tris [pH 8.0], 1 mM EDTA, 1,000 mM KCl, 100 mM $MgCl_2$), 1 μL of purified DICER, 1 μL of 10 mM DTT, 0.5 μL of recombinant RNase inhibitor (Takara; 5,000 U), prelet-7a miRNA (20 to 40 ng), and ultrapure water. Reactions were incubated for 0 to 90 min on a thermocycler followed by addition of 2× TBE-urea loading dye and separation on a 15% TBE-urea gel. Images were visualized on a Licor Odyssey Fc Imaging System in the 700 channel.

Adenoassociated Vector Design, Production, and Delivery. AAV2-hRPE(0.8)-iCre-WPRE and AAV2-CMV-null were obtained from Vector Biolabs. To generate the OptiDicer virus, first Δhel-DICER1 cDNA was cloned into pAAV-MCS (Agilent Technologies). The total packaging genome size to 5.0 kb. The indicated plasmids were transfected into HeLa (ATCC) and primary human retinal pigmented epithelial cells (hRPE) (Lonza), maintained in RtEBM (Lonza) following the manufacturer's instructions. Nucleofection with Basic Epithelial Cells Nucleofector Kit (Lonza) was used for transient plasmid transfection with program U-023. The transfection efficiency was >80% as determined by pMaxGFP transfection with fluorescence microscopy. let-7–resistant DICER1 and OptiDicer were synthesized by GeneArt Gene Synthesis (Thermo Fisher Scientific). Expression of OptiDicer was driven by CMV promoter and contained an SV40 polyadenylation signal in the 3′ end. Production and purification of AAV2-OptiDicer were accomplished by Vigene Biosciences.

Intraocular Injections. Subretinal injections and intravitreous injections (1 μL each) were performed with a 35-gauge Exmire microsyringe (Ito Corporation). The VEGF neutralizing antibody B20-4.1.1 or an equivalent mass of isotype antibody, both provided by Genentech, were delivered by intravitreous injection (0.5 to 1 μg). One microliter of 10^{11} viral genomes (vg)/mL (or 10^8 vg/μL) of AAV-OptiDicer, or AAV2-CMV-null were delivered by subretinal injection. Separately, AAV2-hRPE(0.8)-iCre-WPRE was delivered at by intravitreous injection at 10^{10} genome copies in 1 μL.

Data Availability Statement. The OptiDicer sequence reported in this paper has been deposited in GenBank (https://www.ncbi.nlm.nih.gov/genbank/), accession number MN910264. All data needed to evaluate the conclusions in this paper are available in the main text and the supplementary materials. Requests for additional data discussed in this paper will be made available to readers upon request.

ACKNOWLEDGMENTS. We thank G. Pattison, K. Langberg, D. Robertson, X. Zhou, K. Atwood, and H. Hall for their technical assistance. These studies were supported by NIH Grant R01EY028027 and American Heart Association Grant 13SDG16770008 (B.D.G.); J.A. was supported by NIH Grants DP1GM114862, R01EY022238, R01EY024068, R01EY028027, and R01EY029799; John Templeton Foundation Grant 60763; and the DuPont Guerry, III, Professorship; N.K. by NIH Grants K99EY024336 and R00EY024336; R.D.M. by NIH Grant T32 HL007284; B.K.A. and H.U. by NIH Grants R01EY017950 and R01EY017182; and B.C. by NIH Grant R01EY019943. The content is solely the responsibility of the authors and does not necessarily represent the official views of the NIH.

1. W. L. Wong *et al.*, Global prevalence of age-related macular degeneration and disease burden projection for 2020 and 2040: A systematic review and meta-analysis. *Lancet Glob. Health* **2**, e106–e116 (2014).
2. J. S. Sunness, J. Gonzalez-Baron, N. M. Bressler, B. Hawkins, C. A. Applegate, The development of choroidal neovascularization in eyes with the geographic atrophy form of age-related macular degeneration. *Ophthalmology* **106**, 910–919 (1999).
3. P. Kaszubski, T. Ben Ami, C. Saade, R. T. Smith, Geographic atrophy and choroidal neovascularization in the same eye: A review. *Ophthalmic Res.* **55**, 185–193 (2016).
4. E. Bernstein, A. A. Caudy, S. M. Hammond, G. J. Hannon, Role for a bidentate ribonuclease in the initiation step of RNA interference. *Nature* **409**, 363–366 (2001).
5. J. Gan *et al.*, Structural insight into the mechanism of double-stranded RNA processing by ribonuclease III. *Cell* **124**, 355–366 (2006).
6. Z. Du, J. K. Lee, R. Tjhen, R. M. Stroud, T. L. James, Structural and biochemical insights into the dicing mechanism of mouse Dicer: A conserved lysine is critical for dsRNA cleavage. *Proc. Natl. Acad. Sci. U.S.A.* **105**, 2391–2396 (2008).
7. S. Dridi *et al.*, ERK1/2 activation is a therapeutic target in age-related macular degeneration. *Proc. Natl. Acad. Sci. U.S.A.* **109**, 13781–13786 (2012).
8. B. D. Gelfand *et al.*, Iron toxicity in the retina requires Alu RNA and the NLRP3 inflammasome. *Cell Rep.* **11**, 1686–1693 (2015).
9. H. Kaneko *et al.*, DICER1 deficit induces Alu RNA toxicity in age-related macular degeneration. *Nature* **471**, 325–330 (2011).
10. Y. Kim *et al.*, DICER1/Alu RNA dysmetabolism induces Caspase-8-mediated cell death in age-related macular degeneration. *Proc. Natl. Acad. Sci. U.S.A.* **111**, 16082–16087 (2014).
11. V. Tarallo *et al.*, DICER1 loss and Alu RNA induce age-related macular degeneration via the NLRP3 inflammasome and MyD88. *Cell* **149**, 847–859 (2012).
12. Y. K. Kim, B. Kim, V. N. Kim, Re-evaluation of the roles of DROSHA, Export in 5, and DICER in microRNA biogenesis. *Proc. Natl. Acad. Sci. U.S.A.* **113**, E1881–E1889 (2016).
13. J. E. Babiarz, J. G. Ruby, Y. Wang, D. P. Bartel, R. Blelloch, Mouse ES cells express endogenous shRNAs, siRNAs, and other Microprocessor-independent, Dicer-dependent small RNAs. *Genes Dev.* **22**, 2773–2785 (2008).
14. Q. Hu *et al.*, DICER- and AGO3-dependent generation of retinoic acid-induced DR2 Alu RNAs regulates human stem cell proliferation. *Nat. Struct. Mol. Biol.* **19**, 1168–1175 (2012).
15. Y. F. Ren *et al.*, Dicer-dependent biogenesis of small RNAs derived from 7SL RNA. *PLoS One* **7**, e40705 (2012).
16. Y. Ohnishi *et al.*, Active role of small non-coding RNAs derived from SINE/B1 retrotransposon during early mouse development. *Mol. Biol. Rep.* **39**, 903–909 (2012).
17. M. Flemr *et al.*, A retrotransposon-driven dicer isoform directs endogenous small interfering RNA production in mouse oocytes. *Cell* **155**, 807–816 (2013).
18. E. P. Murchison *et al.*, Critical roles for Dicer in the female germline. *Genes Dev.* **21**, 682–693 (2007).
19. N. Kerur *et al.*, TLR-independent and P2X7-dependent signaling mediate Alu RNA-induced NLRP3 inflammasome activation in geographic atrophy. *Invest. Ophthalmol. Vis. Sci.* **54**, 7395–7401 (2013).
20. N. Kerur *et al.*, cGAS drives noncanonical-inflammasome activation in age-related macular degeneration. *Nat. Med.* **24**, 50–61 (2018).
21. B. J. Fowler *et al.*, Nucleoside reverse transcriptase inhibitors possess intrinsic anti-inflammatory activity. *Science* **346**, 1000–1003 (2014).
22. E. Bernstein *et al.*, Dicer is essential for mouse development. *Nat. Genet.* **35**, 215–217 (2003).
23. W. J. Yang *et al.*, Dicer is required for embryonic angiogenesis during mouse development. *J. Biol. Chem.* **280**, 9330–9335 (2005).
24. T. R. Sundermeier *et al.*, MicroRNA-processing enzymes are essential for survival and function of mature retinal pigmented epithelial cells in mice. *J. Biol. Chem.* **292**, 3366–3378 (2017).
25. M. Otsuka *et al.*, Hypersusceptibility to vesicular stomatitis virus infection in Dicer1-deficient mice is due to impaired miR24 and miR93 expression. *Immunity* **27**, 123–134 (2007).
26. E. Ostermann *et al.*, Deregulation of type I IFN-dependent genes correlates with increased susceptibility to cytomegalovirus acute infection of dicer mutant mice. *PLoS One* **7**, e43744 (2012).

27. M. Otsuka *et al*., Impaired microRNA processing causes corpus luteum insufficiency and infertility in mice. *J. Clin. Invest.* **118**, 1944–1954 (2008).
28. E. Ostermann, C. Macquin, W. Krezel, S. Bahram, P. Georgel, Increased viral dissemination in the brain and lethality in MCMV-infected, dicer-deficient neonates. *Viruses* **7**, 2308–2320 (2015).
29. G. Alsaleh *et al*., Reduced DICER1 expression bestows rheumatoid arthritis synoviocytes proinflammatory properties and resistance to apoptotic stimuli. *Arthritis Rheumatol.* **68**, 1839–1848 (2016).
30. M. J. Mattapallil *et al*., The Rd8 mutation of the Crb1 gene is present in vendor lines of C57BL/6N mice and embryonic stem cells, and confounds ocular induced mutant phenotypes. *Invest. Ophthalmol. Vis. Sci.* **53**, 2921–2927 (2012).
31. C. A. Curcio, Soft drusen in age-related macular degeneration: Biology and targeting via the oil spill strategies. *Invest. Ophthalmol. Vis. Sci.* **59**, AMD160–AMD181 (2018).
32. R. Hoerster *et al*., In-vivo and ex-vivo characterization of laser-induced choroidal neovascularization variability in mice. *Graefes Arch. Clin. Exp. Ophthalmol.* **250**, 1579–1586 (2012).
33. H. G. Yu *et al*., Increased choroidal neovascularization following laser induction in mice lacking lysyl oxidase-like 1. *Invest. Ophthalmol. Vis. Sci.* **49**, 2599–2605 (2008).
34. M. Fukasawa *et al*., Genomic imprinting in Dicer1-hypomorphic mice. *Cytogenet. Genome Res.* **113**, 138–143 (2006).
35. S. Morita *et al*., Dicer is required for maintaining adult pancreas. *PLoS One* **4**, e4212 (2009).
36. B. D. Harfe, M. T. McManus, J. H. Mansfield, E. Hornstein, C. J. Tabin, The RNaseIII enzyme Dicer is required for morphogenesis but not patterning of the vertebrate limb. *Proc. Natl. Acad. Sci. U.S.A.* **102**, 10898–10903 (2005).
37. E. Hasegawa *et al*., Characterization of a spontaneous retinal neovascular mouse model. *PLoS One* **9**, e106507 (2014).
38. N. Nagai *et al*., Spontaneous CNV in a novel mutant mouse is associated with early VEGF-A-driven angiogenesis and late-stage focal edema, neural cell loss, and dysfunction. *Invest. Ophthalmol. Vis. Sci.* **55**, 3709–3719 (2014).
39. B. Chang *et al*., Spontaneous posterior segment vascular disease phenotype of a mouse model, rnv3, is dependent on the Crb1rd8 allele. *Invest. Ophthalmol. Vis. Sci.* **59**, 5127–5139 (2018).
40. R. Foxton, A. Osborne, K. R. Martin, Y. S. Ng, D. T. Shima, Distal retinal ganglion cell axon transport loss and activation of p38 MAPK stress pathway following VEGF-A antagonism. *Cell Death Dis.* **7**, e2212 (2016).
41. N. Nagai *et al*., Novel CCR3 antagonists are effective mono- and combination inhibitors of choroidal neovascular growth and vascular permeability. *Am. J. Pathol.* **185**, 2534–2549 (2015).
42. L. Paneghetti, Y. S. Ng, A novel endothelial-derived anti-inflammatory activity significantly inhibits spontaneous choroidal neovascularisation in a mouse model. *Vasc. Cell* **8**, 2 (2016).
43. J. W. Bainbridge *et al*., Effect of gene therapy on visual function in Leber's congenital amaurosis. *N. Engl. J. Med.* **358**, 2231–2239 (2008).
44. A. M. Maguire *et al*., Safety and efficacy of gene transfer for Leber's congenital amaurosis. *N. Engl. J. Med.* **358**, 2240–2248 (2008).
45. S. H. Lee *et al*., Transduction patterns of adeno-associated viral vectors in a laser-induced choroidal neovascularization mouse model. *Mol. Ther. Methods Clin. Dev.* **9**, 90–98 (2018).
46. G. Schnabolk *et al*., Delivery of CR2-fH using AAV vector therapy as treatment strategy in the mouse model of choroidal neovascularization. *Mol. Ther. Methods Clin. Dev.* **9**, 1–11 (2017).
47. Y. Sun *et al*., Inflammatory signals from photoreceptor modulate pathological retinal angiogenesis via c-Fos. *J. Exp. Med.* **214**, 1753–1767 (2017).
48. Y. Sun *et al*., Sema3f protects against subretinal neovascularization in vivo. *EBioMedicine* **18**, 281–287 (2017).
49. L. Luo *et al*., Photoreceptor avascular privilege is shielded by soluble VEGF receptor-1. *eLife* **2**, e00324 (2013).
50. C. M. Lai *et al*., Long-term evaluation of AAV-mediated sFlt-1 gene therapy for ocular neovascularization in mice and monkeys. *Mol. Ther.* **12**, 659–668 (2005).
51. J. Y. Dong, P. D. Fan, R. A. Frizzell, Quantitative analysis of the packaging capacity of recombinant adeno-associated virus. *Hum. Gene Ther.* **7**, 2101–2112 (1996).
52. Z. Wu, H. Yang, P. Colosi, Effect of genome size on AAV vector packaging. *Mol. Ther.* **18**, 80–86 (2010).
53. E. Ma, I. J. MacRae, J. F. Kirsch, J. A. Doudna, Autoinhibition of human dicer by its internal helicase domain. *J. Mol. Biol.* **380**, 237–243 (2008).
54. A. M. Gurtan, V. Lu, A. Bhutkar, P. A. Sharp, In vivo structure-function analysis of human Dicer reveals directional processing of precursor miRNAs. *RNA* **18**, 1116–1122 (2012).
55. E. M. Kennedy *et al*., Production of functional small interfering RNAs by an amino-terminal deletion mutant of human Dicer. *Proc. Natl. Acad. Sci. U.S.A.* **112**, E6945–E6954 (2015).
56. I. J. MacRae, K. Zhou, J. A. Doudna, Structural determinants of RNA recognition and cleavage by Dicer. *Nat. Struct. Mol. Biol.* **14**, 934–940 (2007).
57. J. B. Ma, K. Ye, D. J. Patel, Structural basis for overhang-specific small interfering RNA recognition by the PAZ domain. *Nature* **429**, 318–322 (2004).
58. X. H. Liang, C. E. Hart, S. T. Crooke, Transfection of siRNAs can alter miRNA levels and trigger non-specific protein degradation in mammalian cells. *Biochim. Biophys. Acta* **1829**, 455–468 (2013).
59. J. J. Forman, A. Legesse-Miller, H. A. Coller, A search for conserved sequences in coding regions reveals that the let-7 microRNA targets Dicer within its coding sequence. *Proc. Natl. Acad. Sci. U.S.A.* **105**, 14879–14884 (2008).
60. X. Wang, miRDB: A microRNA target prediction and functional annotation database with a wiki interface. *RNA* **14**, 1012–1017 (2008).
61. N. Wong, X. Wang, miRDB: An online resource for microRNA target prediction and functional annotations. *Nucleic Acids Res.* **43**, D146–D152 (2015).
62. X. Zhang *et al*., AAV2 delivery of Flt23k intraceptors inhibits murine choroidal neovascularization. *Mol. Ther.* **23**, 226–234 (2015).
63. S. E. Barker *et al*., Subretinal delivery of adeno-associated virus serotype 2 results in minimal immune responses that allow repeat vector administration in immunocompetent mice. *J. Gene Med.* **11**, 486–497 (2009).
64. M. Carido *et al*., Characterization of a mouse model with complete RPE loss and its use for RPE cell transplantation. *Invest. Ophthalmol. Vis. Sci.* **55**, 5431–5444 (2014).
65. J. Wang, J. Iacovelli, C. Spencer, M. Saint-Geniez, Direct effect of sodium iodate on neurosensory retina. *Invest. Ophthalmol. Vis. Sci.* **55**, 1941–1953 (2014).
66. Y. Suárez *et al*., Dicer-dependent endothelial microRNAs are necessary for postnatal angiogenesis. *Proc. Natl. Acad. Sci. U.S.A.* **105**, 14082–14087 (2008).
67. A. Kuehbacher, C. Urbich, A. M. Zeiher, S. Dimmeler, Role of Dicer and Drosha for endothelial microRNA expression and angiogenesis. *Circ. Res.* **101**, 59–68 (2007).
68. S. Chen *et al*., Global microRNA depletion suppresses tumor angiogenesis. *Genes Dev.* **28**, 1054–1067 (2014).
69. P. N. Plummer *et al*., MicroRNAs regulate tumor angiogenesis modulated by endothelial progenitor cells. *Cancer Res.* **73**, 341–352 (2013).
70. Y. Li *et al*., MicroRNA-107 contributes to post-stroke angiogenesis by targeting Dicer-1. *Sci. Rep.* **5**, 13316 (2015).
71. J. A. Hanna *et al*., Biallelic *Dicer1* loss mediated by *aP2-Cre* drives angiosarcoma. *Cancer Res.* **77**, 6109–6118 (2017).
72. Y. Fan *et al*., Dicer suppresses the malignant phenotype in VHL-deficient clear cell renal cell carcinoma by inhibiting HIF-2α. *Oncotarget* **7**, 18280–18294 (2016).
73. Y. S. Chen *et al*., Dicer suppresses MMP-2-mediated invasion and VEGFA-induced angiogenesis and serves as a promising prognostic biomarker in human clear cell renal cell carcinoma. *Oncotarget* **7**, 84299–84313 (2016).
74. M. Grunin, T. Burstyn-Cohen, S. Hagbi-Levi, A. Peled, I. Chowers, Chemokine receptor expression in peripheral blood monocytes from patients with neovascular age-related macular degeneration. *Invest. Ophthalmol. Vis. Sci.* **53**, 5292–5300 (2012).
75. Y. Imamura *et al*., Drusen, choroidal neovascularization, and retinal pigment epithelium dysfunction in SOD1-deficient mice: A model of age-related macular degeneration. *Proc. Natl. Acad. Sci. U.S.A.* **103**, 11282–11287 (2006).
76. J. Ambati *et al*., An animal model of age-related macular degeneration in senescent Ccl-2- or Ccr-2-deficient mice. *Nat. Med.* **9**, 1390–1397 (2003).
77. K. Kuida *et al*., Altered cytokine export and apoptosis in mice deficient in interleukin-1 beta converting enzyme. *Science* **267**, 2000–2003 (1995).
78. H. Wei, Z. Xun, H. Granado, A. Wu, J. T. Handa, An easy, rapid method to isolate RPE cell protein from the mouse eye. *Exp. Eye Res.* **145**, 450–455 (2016).
79. M. Fareh *et al*., TRBP ensures efficient Dicer processing of precursor microRNA in RNA-crowded environments. *Nat. Commun.* **7**, 13694 (2016).
80. J. E. Park *et al*., Dicer recognizes the 5′ end of RNA for efficient and accurate processing. *Nature* **475**, 201–205 (2011).